Environment International 131 (2019) 105027

Contents lists available at ScienceDirect

Environment International

journal homepage: www.elsevier.com/locate/envint

Predicted temperature-increase-induced global health burden and its regional variability

Jae Young Lee[a], Ho Kim[a,*], Antonio Gasparrini[b], Ben Armstrong[b], Michelle L. Bell[c], Francesco Sera[b], Eric Lavigne[d,e], Rosana Abrutzky[f], Shilu Tong[g,h,i], Micheline de Sousa Zanotti Stagliorio Coelho[j,k], Paulo Hilario Nascimento Saldiva[j], Patricia Matus Correa[l], Nicolas Valdes Ortega[l], Haidong Kan[m,n], Samuel Osorio Garcia[o], Jan Kyselý[p,q], Aleš Urban[p], Hans Orru[r,s], Ene Indermitte[r], Jouni J.K. Jaakkola[t], Niilo R.I. Ryti[t], Mathilde Pascal[u], Patrick G. Goodman[v], Ariana Zeka[w], Paola Michelozzi[x], Matteo Scortichini[x], Masahiro Hashizume[y], Yasushi Honda[z], Magali Hurtado[aa], Julio Cruz[aa], Xerxes Seposo[ab], Baltazar Nunes[ac], João Paulo Teixeira[ac,ad], Aurelio Tobias[ae], Carmen Íñiguez[af], Bertil Forsberg[ag], Christofer Åström[ag], Ana Maria Vicedo-Cabrera[b], Martina S. Ragettli[ah,ai], Yue-Liang Leon Guo[aj], Bing-Yu Chen[aj], Antonella Zanobetti[ak], Joel Schwartz[ak], Tran Ngoc Dang[al,am], Dung Do Van[al], Fetemeh Mayvaneh[an], Ala Overcenco[ao], Shanshan Li[ap,aq], Yuming Guo[ap,aq]

[a] Graduate School of Public Health, Institute of Health and Environment, Seoul National University, Seoul, Republic of Korea
[b] Department of Social and Environmental Health Research, London School of Hygiene & Tropical Medicine, London, UK
[c] School of Forestry and Environmental Studies, Yale University, New Haven, CT, USA
[d] Air Health Science Division, Health Canada, Ottawa, ON, Canada
[e] School of Epidemiology & Public Health, University of Ottawa, Ottawa, ON, Canada
[f] Universidad de Buenos Aires, Facultad de Ciencias Sociales, Instituto de Investigaciones Gino Germani, Buenos Aires, Argentina
[g] School of Public Health, Institute of Environment and Human Health, Anhui Medical University, Hefei, China
[h] Shanghai Children's Medical Centre, Shanghi Jiao-Tong University, Shanghai, China
[i] School of Public Health and Social Work, Queensland University of Technology, Brisbane, QLD, Australia
[j] Institute of Advanced Studies of the University of São Paulo, São Paulo, Brazil
[k] Climate Change Cluster, Faculty of Sciences, University of Technology–Sydney, Sydney, Australia
[l] Department of Public Health, Universidad de los Andes, Santiago, Chile
[m] School of Public Health, Key Lab of Public Health Safety of the Ministry of Education, Key Lab of Health Technology Assessment of the Ministry of Health, Fudan University, Shanghai, China
[n] Shanghai Key Laboratory of Atmospheric Particle Pollution and Prevention (LAP3), Fudan University, Shanghai, China
[o] Hospital Vista Hermosa, Bogotá, Colombia
[p] Institute of Atmospheric Physics, Czech Academy of Sciences, Prague, Czech Republic
[q] Faculty of Environmental Sciences, Czech University of Life Sciences, Prague, Czech Republic
[r] Institute of Family Medicine and Public Health, University of Tartu, Tartu, Estonia
[s] Department of Public Health and Clinical Medicine, Umeå University, Umeå, Sweden
[t] Center for Environmental and Respiratory Health Research, University of Oulu, Oulu, Finland
[u] Santé Publique France, French National Public Health Agency, Saint Maurice, France
[v] School of Physics, Dublin Institute of Technology, Dublin, Ireland
[w] Institute of Environment, Health and Societies, Brunel University London, London, UK
[x] Department of Epidemiology, Lazio Regional Health Service, Rome, Italy
[y] Department of Pediatric Infectious Diseases, Institute of Tropical Medicine, Nagasaki University, Nagasaki, Japan
[z] Faculty of Health and Sport Science, University of Tsukuba, Tsukuba, Japan
[aa] Department of Environmental Health, National Institute of Public Health, Cuernavaca, Morelos, Mexico
[ab] Department of Environmental Engineering, Kyoto University, Kyoto, Japan
[ac] Department of Epidemiology, Instituto Nacional de Saúde Dr. Ricardo Jorge, Lisboa, Portugal
[ad] EPIUnit – Instituto de Saúde Pública, Universidade do Porto, Porto, Portugal
[ae] Institute of Environmental Assessment and Water Research, Spanish Council for Scientific Research, Barcelona, Spain
[af] Department of Statistics and Computational Research, University of Valencia, Environmental Health Joint Research Unit FiSABIO-UV-UJI CIBERESP, Spain
[ag] Department of Public Health and Clinical Medicine, Umeå University, Umeå, Sweden
[ah] Swiss Tropical and Public Health Institute, Basel, Switzerland
[ai] University of Basel, Basel, Switzerland

* Corresponding author.
E-mail address: hokim@snu.ac.kr (H. Kim).

https://doi.org/10.1016/j.envint.2019.105027

[aj] Environmental and Occupational Medicine, National Taiwan University, NTU Hospital, Taipei, Taiwan
[ak] Department of Environmental Health, Harvard T.H. Chan School of Public Health, Boston, MA, USA
[al] Faculty of Public Health, University of Medicine and Pharmacy of Ho Chi Minh City, Ho Chi Minh City, Viet Nam
[am] The Institute of Research and Development, Duy Tan University, Da Nang, Viet Nam
[an] Faculty of Geography and Environmental Sciences, Hakim Sabzevari University, Sabzevar 9617916487, Khorasan Razavi, Iran
[ao] Laboratory of Management in Science and Public Health, National Agency for Public Health of the Ministry of Health of R. Moldova, Chisinau, Republic of Moldova
[ap] Climate, Air Quality Research Unit, School of Public Health and Preventive Medicine, Monash University, Melbourne, Australia
[aq] Department of Epidemiology and Preventive Medicine, School of Public Health and Preventive Medicine, Monash University, Melbourne, Australia

ARTICLE INFO

Handling Editor: Zorana Jovanovic Andersen

Keywords:
Projection
Mortality
Climate change
Regional variation
Vulnerability

ABSTRACT

An increase in the global health burden of temperature was projected for 459 locations in 28 countries worldwide under four representative concentration pathway scenarios until 2099. We determined that the amount of temperature increase for each 100 ppm increase in global CO_2 concentrations is nearly constant, regardless of climate scenarios. The overall average temperature increase during 2010–2099 is largest in Canada (1.16 °C/100 ppm) and Finland (1.14 °C/100 ppm), while it is smallest in Ireland (0.62 °C/100 ppm) and Argentina (0.63 °C/100 ppm). In addition, for each 1 °C temperature increase, the amount of excess mortality is increased largely in tropical countries such as Vietnam (10.34%p/°C) and the Philippines (8.18%p/°C), while it is decreased in Ireland (−0.92%p/°C) and Australia (−0.32%p/°C). To understand the regional variability in temperature increase and mortality, we performed a regression-based modeling. We observed that the projected temperature increase is highly correlated with daily temperature range at the location and vulnerability to temperature increase is affected by health expenditure, and proportions of obese and elderly population.

1. Introduction

The global concentration of carbon dioxide is a major factor in determining the magnitude of future climate change and resulting effects on human health (Intergovernmental Panel on Climate Change (IPCC), 2007). One of the important pathways by which carbon dioxide affects human health is through the greenhouse effect, which increases the atmospheric temperature and consequently affects temperature-attributable excess mortality (Liu et al., 2011; Patz et al., 2000). This causal link has been characterized by many previous studies in many regions of the world, showing that the health burden of elevated temperature is determined by the net effect of increased heat-related mortality and decreased cold-related mortality (Błażejczyk et al., 2013; Gasparrini et al., 2017; Guo et al., 2016; Hajat et al., 2014; Lee and Kim, 2016; Lee et al., 2018; Li et al., 2013; Martin et al., 2012; Schwartz et al., 2015; Vardoulakis et al., 2014).

According to previous studies, the net health burden of temperature increase varies across the globe, and there are regions where populations are much more vulnerable to temperature increase. Gasparrini et al. (2017) projected temperature-related excess mortality under representative concentration pathway (RCP) scenarios until 2099 for 451 locations in 23 countries. This study demonstrated that Northern Europe, East Asia, and Australia are estimated to experience marginally negative net excess mortality change in 2090 compared with 2010 under RCP 8.5, while Americas, Central and Southern Europe, and Southeast Asia are anticipated to experience positive net excess mortality change. The excess mortality across the nine continental regions of the world ranged from −1.2% (in Australia) to 12.7% (in Southeast Asia). The regional trends of temperature-related mortality under other scenarios are somewhat different. For example, all regions showed nearly null or very small net effect under RCP 2.6, and Central America showed negative net effect in 2090 under RCP 4.5 unlike the positive net effect under RCP 8.5. Understanding the cause of the regional variation is critical to developing the best policies to protect public health in the present day and under a changing climate, especially for vulnerable regions. However, little is known about the factors and mechanisms that contribute to regional differences.

This study projected temperature-related mortality under RCP scenarios until 2099 for 459 locations in 28 countries using the database collected through the Multi-City Multi-Country (MCC) Collaborative Research Network. To represent the health impact of temperature increase in these locations, we formulated indices for temperature increase, vulnerability, and mortality increase, i.e. the temperature increase related to global CO_2 concentration increase, mortality increase related to temperature increase, and mortality increase related to global CO_2 concentration increase. These indices represent the normalized effects of climate change with a single value invariant to the baseline periods, projections periods, and climate scenarios. Based on these indices, we aimed to compare the regional differences in temperature increase risks and analyze the factors that affect the future temperature-related mortality. To best of our knowledge, this is the first paper to analyze the factors that affect the regional variability of future temperature-related mortality in global scale.

2. Methods

2.1. Data collection

Historical data including daily non-external (ICD-10 A00-R99) or all-cause mortality and daily mean temperature for 459 locations in 28 countries were obtained through MCC Collaborative Research Network (http://mccstudy.lshtm.ac.uk). Supplementary Tables S1 and S2 show the description and descriptive statistics of the data. Supplementary Fig. S1 shows the map of the 459 locations.

Location-specific daily mean temperature projection data until 2099 were based on the projection data developed by the Inter-Sectoral Impact Model Intercomparison Project for five general circulation models (GFDL-ESM2M, HadGEM2-ES, IPSL-CM5A-LR, MIROC-ESM-CHEM, and NorESM1-M) and four representative concentration pathways (RCP 2.6, RCP 4.5, RCP 6.0, and RCP 8.5), in 0.5° × 0.5° spatial resolution (Warszawski et al., 2014). RCP 8.5 is a business-as-usual greenhouse gas emissions scenario, which leads to a radiative forcing of 8.5 W/m^2 at 2100, while RCP 2.6, RCP 4.5 and RCP 6.0 are mitigation scenarios, which lead to a radiative forcing of 2.6, 4.5, and 6.0 W/m^2 at 2100, respectively. We obtained the modeled temperature series of the corresponding grid cell for each location and recalibrated them using the observed series so that both series have the same monthly and interdiurnal temperature variabilities during the baseline period (Hempel et al., 2013).

In addition to the historical and projected temperature data, location-specific meta-variables were collected from various sources. Köppen-Geiger climatological zone was obtained from MCC, distance to the nearest coast were extracted from Natural Earth's coastline data (https://www.naturalearthdata.com), total annual health expenditure

per capita and population proportion aged 65 and over were obtained from World Bank (https://data.worldbank.org), and population proportions below poverty line and with obesity were obtained from Central Intelligence Agency (https://www.cia.gov/library/publications/the-world-factbook). Year of information for the health expenditure and population proportions was summarized in Table S3.

2.2. Temperature-mortality relationship assessment

We estimated the location-specific temperature-mortality relationship using the historical temperature and mortality data based on the two-stage time series analysis described in previous studies (Gasparrini et al., 2017; Gasparrini et al., 2015). In the first stage, we estimated the relationship for each location using distributed lag nonlinear model (Gasparrini et al., 2010), which is expressed as follows:

$$\log(E[\text{Mortality}]) = CB + DOW + NS(\text{time}) \quad (1)$$

Here, quasi-Poisson distribution is assumed for the mortality, and CB is a cross-basis of lagged temperature effect with lags modeled up to 21 days. For the cross-basis, the temperature-mortality curve was modeled with a natural cubic B-spline with three internal knots at the 10th, 75th, and 90th percentiles of regional temperature (4 degrees of freedom) and the lag-mortality curve with a natural cubic B-spline with an intercept and three logarithmically equally spaced internal knots (5 degrees of freedom) (Gasparrini et al., 2015). DOW is day of the week to control for daily variation within a week, and NS (time) is the natural cubic spline of time with 8 degrees of freedom per year to control for the seasonal and long-term variations.

In the second stage, we obtained the best linear unbiased prediction (BLUP) of the estimated temperature-mortality relationship based on the meta-analysis (Bai et al., 2016). The BLUP represents a trade-off between the location-specific and pooled relationships to allow locations with small daily mortality counts to borrow information from the pooled relationships (Gasparrini et al., 2012). Köppen-Geiger climatological zone, continent indicator, and daily mean temperature were selected as predictors in the meta-analysis based on Akaike information criterion (Akaike, 1974). Supplementary Table S4 shows various meta-analysis models and their corresponding Akaike information criterion (AIC) and I^2 values. This stage produces an overall estimate of the association between temperature and mortality for each city.

2.3. Excess mortality projection

To project the excess mortality attributable to future temperature, we averaged five GCM temperature series for each location and each RCP scenario to average out the prediction uncertainty and extreme behavior of a certain GCM. The monthly and interdiurnal temperature variabilities of the GCM-ensemble series were recalibrated using the observed series (Hempel et al., 2013). Then, we obtained the daily relative risk of GCM-ensemble temperature based on the temperature-mortality relationship. The location-specific excess mortality is calculated using the following equation:

$$EM_j = \frac{TAM_j}{NTAM_j} = \frac{\sum_{i=1}^{n} (RR_{i,j} - 1)}{n} \quad (2)$$

Here, EM_j is the excess mortality attributable to temperature for location j, TAM_j is the temperature-attributable mortality for location j, $NTAM_j$ is the non-temperature-attributable mortality for location j, $RR_{i,j}$ is the relative risk of mortality due to temperature predicted by BLUP in the second stage for day i and location j, and n is the total number of days in the projection period. The heat- and cold-related portions of mortality are defined respectively as follows:

$$EM_{heat,j} = \frac{\sum_i (RR_{i,j} - 1)}{n} \text{ for i which } T_i \geq MMT \quad (3)$$

$$EM_{cold,j} = \frac{\sum_i (RR_{i,j} - 1)}{n} \text{ for i which } T_i < MMT \quad (4)$$

Here, T_i is the temperature for day i, n is the total number of days in the projection period, and MMT is the minimum mortality temperature (Tobias et al., 2017). The excess mortality for continent or country with multiple study locations can be calculated as follows:

$$EM = \frac{\sum_j (TAM_j)}{\sum_j (NTAM_j)} = \frac{\sum_j (EM_j \bullet NTAM_j)}{\sum_j (NTAM_j)} \quad (5)$$

2.4. Descriptive indices calculation

We defined three descriptive indices for temperature-increase-induced health burden: *Temperature increase index* is the regional temperature increase per 100 ppm increase of global CO_2 concentration (°C/100 ppm), *vulnerability index* is the percent point increase of regional excess mortality per 1 °C increase of regional temperature (%p/°C), and *mortality increase index* is the percent point increase of regional excess mortality per 100 ppm increase of global CO_2 concentration (%p/100 ppm). All three indices were obtained for each location by applying linear regressions to the projection data aggregated for the period of 2010–2099 and four RCPs.

2.5. Feature selection and index modeling

To understand the regional variability in temperature increase index, we performed multiple penalized nonlinear regressions using generalized additive models (Wood, 2006). Factors in the models were selected based on the full brute-force method, in which we evaluated all possible combinations of location-specific range of daily temperatures (defined as the difference between 90 and 10 percentile temperatures), daily mean temperature, and distance to the nearest coast. Among the combinations, the best set of factors was selected based on AIC. The relationships with the indices and the selected factors were obtained from the regression result.

Similarly, we analyzed the regional variability in vulnerability index. In addition to the above three factors, we evaluated country-specific demographic and socio-economic factors via the full brute-force method for modeling. Demographic factors were population proportions below poverty line, aged 65 and over, and with obesity, and socio-economic factor was the total health expenditure per capita. The use of such country-specific factors may increase the possibility of overfitting, since the number of data in a country-specific factor is only 28, whereas that in a location-specific factor is 459. Therefore, we used a linear model for vulnerability index.

3. Results

In the first sub-section, we presented temperature-mortality-relationship and excess mortality for 459 locations based on the method described in Temperature-mortality relationship assessment and Excess mortality projection sections in Methods. In the second sub-section, we presented temperature-increase-induced health burden. Index calculation method is described in Descriptive index calculation section in Methods. In the last sub-section, we presented feature selection and index modeling based on the method described in Feature selection and index modeling section in Methods.

3.1. Temperature-mortality relationship and excess mortality

We obtained the BLUP of temperature-mortality relationship for 459 locations in 28 countries. The residual heterogeneity represented by an I^2 index was 47.6% (Higgins and Thompson, 2002). Based on the temperature-mortality relationships and future temperature projections, we calculated an estimated increase in excess mortality for 10

continental regions and 28 countries. Supplementary Figs. S2 and S3 show the temperature increase until 2090s under four RCP scenarios for each region and each country, respectively, while Supplementary Figs. S4 and S5 show the projected increase in excess mortality for each region and each country, respectively. Temperature increase is highest for RCP 8.5 and lowest for RCP 2.6, and small variability was observed across locations. For example, temperature increase in 2090s under RCP 8.5 is largest in Canada (5.44 °C) followed by Finland (5.37 °C) and Estonia (5.28 °C) and smallest in Argentina (2.99 °C) followed by Ireland (3.06 °C) and Chile (3.09 °C). The increase in excess mortality shows much larger variability across locations. For example, excess mortality increase in 2090s under RCP 8.5 is large in Vietnam (43.6%

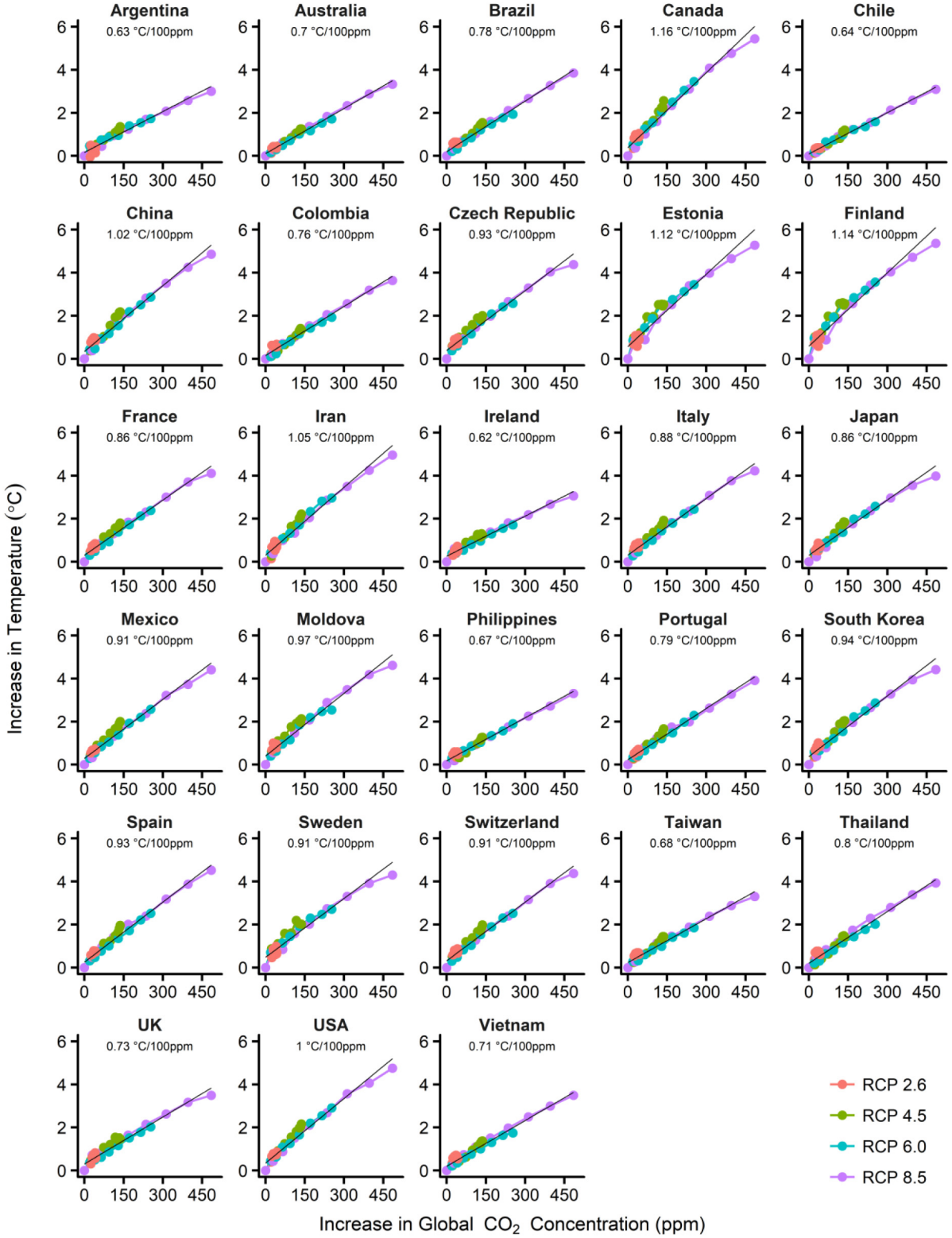

Fig. 1. Temperature increase with respect to global CO_2 concentration increase under four RCP scenarios in 2010–2099 for each country. The top of each panel shows the slope of the linear regression, dubbed as temperature increase index.

p), the Philippines (32.7%p), and Spain (21.6%p), while it is small in Ireland (−2.51%p), Estonia (−0.625%p), and United Kingdom (−0.476%p).

3.2. Temperature-increase-induced health burden

To quantify health burden due to temperature increase, we defined and calculated three descriptive indices related to health burden (see Methods for the definition). We obtained the regional temperature increase averaged over every ten-year period from 2010s (2010–2019) to

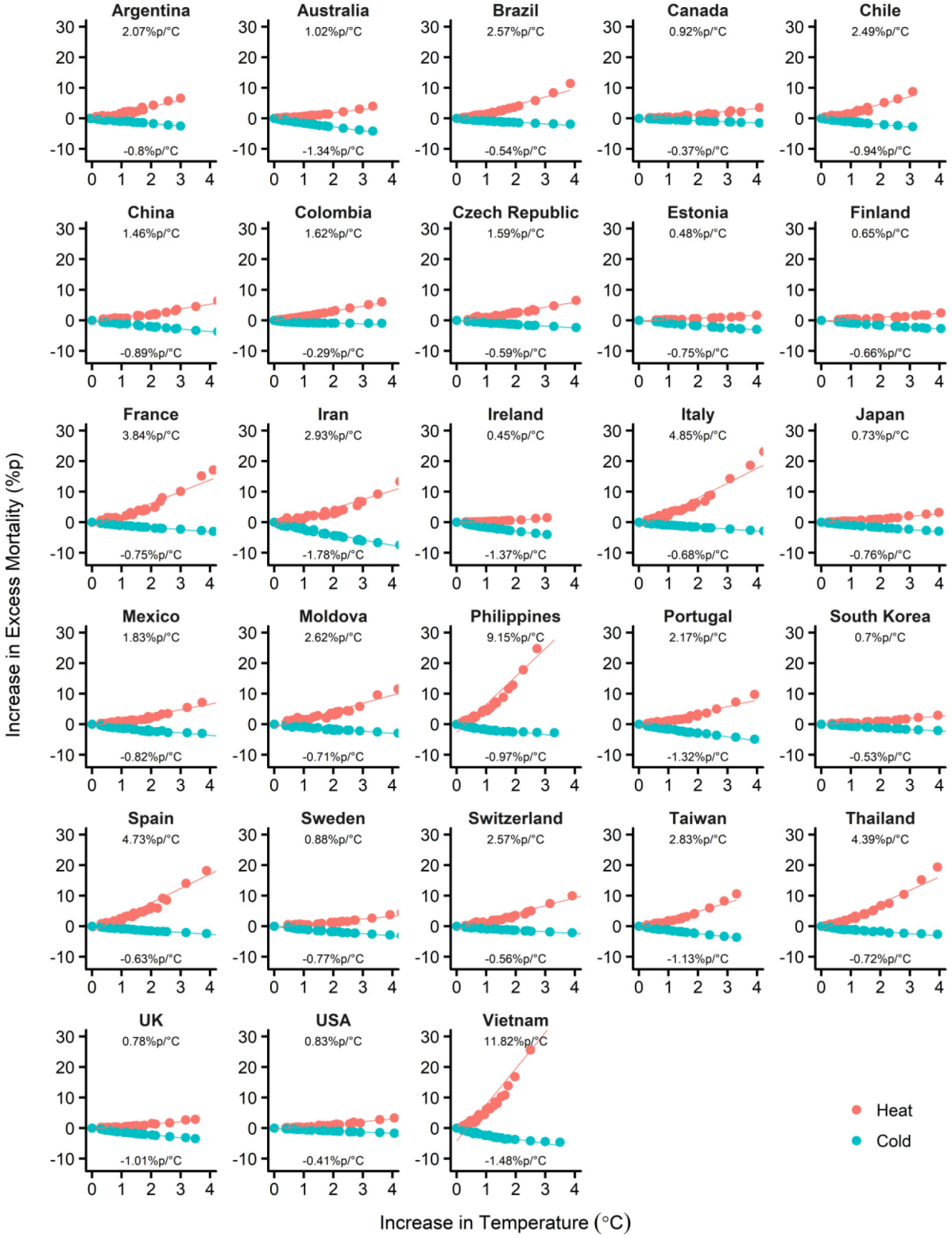

Fig. 2. Heat- and cold-attributable excess mortality with respect to regional temperature increase under four RCP scenarios in 2010–2099 for each country. The top and bottom of each panel show the linear regression slopes of heat-related and cold-related mortality, dubbed as heat and cold vulnerability indices, respectively.

2090s (2090–2099) with respect to global CO_2 concentration increase under four RCP scenarios as shown in Supplementary Fig. S6 and Fig. 1 for each region and each country, respectively. Note that all the points on the graph fall largely on one straight line, so the slope of the linear regression, dubbed as temperature increase index, can represent the entire temperature increase trend of a location regardless of RCP scenarios and projection period. Such linear relationship was similarly observed in Seneviratne et al. (2016). The mean R^2 value of the fit among 28 countries is 0.96, with the minimum R^2 value of 0.93 observed in Finland (Fig. 1). The temperature increase index values were shown at the top side of each panel in Supplementary Fig. S6 and Fig. 1. The index varies across locations, suggesting that temperature increases faster at some locations than others for a given increase of global CO_2. Canada (1.16 °C/100 ppm), Finland (1.14 °C/100 ppm), and Estonia (1.12 °C/100 ppm) were the countries with the highest index, while Ireland (0.62 °C/100 ppm), Argentina (0.63 °C/100 ppm), and Chile (0.64 °C/100 ppm) had the lowest index. The variability of the temperature increase index across 10 regions shown in Supplementary Fig. S6 follows the overall index characteristics of the countries (Fig. 1).

Supplementary Fig. S7 and Fig. 2 show the increase in regional excess mortality due to increase in regional temperature under four RCP scenarios for each region and each country, respectively. Similar to Supplementary Fig. S6 and Fig. 1, the points lie largely on a straight line. The mean R^2 values of the fit among 28 countries were 0.96 for heat vulnerability and 0.88 for cold vulnerability (Fig. 2). The minimum R^2 values were observed in Vietnam (0.93) for heat vulnerability and in Colombia (0.59) for cold vulnerability. The R^2 value for Colombia was small mainly due to a small cold vulnerability of −0.21%p/°C. The red and blue lines represent linear regression results of the heat- and cold-related excess mortality, the slopes of which were dubbed as vulnerability indices for heat and cold. These indices were shown at the top and the bottom of the panel for heat and cold, respectively. The heat vulnerability index is the highest in tropical countries such as Vietnam (11.82%p/°C) and the Philippines (9.15%p/°C), and Southern European countries such as Italy (4.85%p/°C) and Spain (4.73%p/°C). By contrast, the cold vulnerability index is the lowest in Iran (−1.78%p/°C), Vietnam (−1.48%p/°C), and Ireland (−1.37%p/°C).

Lastly, we calculated the estimated heat- and cold-related mortality increase indices from excess mortality increase trend with respect to the global CO_2 concentration increase shown in Supplementary Figs. S8 (region) and S9 (country). The heat- and cold-related indices were displayed at the top and bottom of the panel. The total mortality increase index, the sum of heat- and cold-related mortality increase indices, represents the overall health burden of the global CO_2 increase and was the highest in tropical countries such as Vietnam (7.62%p/100 ppm), the Philippines (5.66%p/100 ppm), and Thailand (3.07%p/100 ppm), and Southern European countries such as Spain (3.95%p/100 ppm) and Italy (3.84%p/100 ppm). The variability in the mortality increase index originated from the variability in temperature increase and vulnerability. To understand what extent the variability in the total mortality increase index depended on those of temperature increase

Table 1
Descriptive indices for each region and each country. See Methods for the definition of three descriptive indices.

	Temperature increase [°C/100 ppm]	Vulnerability [%p/°C]			Mortality increase [%p/100 ppm]		
		Heat	Cold	Total	Heat	Cold	Total
North America	1.03	0.83	−0.40	0.43	0.89	−0.40	0.49
Canada	1.16	0.92	−0.37	0.55	1.13	−0.43	0.70
USA	1.00	0.83	−0.41	0.42	0.87	−0.40	0.47
Central America	0.91	1.83	−0.82	1.00	1.75	−0.72	1.03
Mexico	0.91	1.83	−0.82	1.00	1.75	−0.72	1.03
South America	0.75	2.34	−0.57	1.78	1.80	−0.42	1.38
Argentina	0.63	2.07	−0.80	1.27	1.36	−0.51	0.85
Brazil	0.78	2.57	−0.54	2.03	2.06	−0.42	1.64
Chile	0.64	2.49	−0.94	1.56	1.61	−0.59	1.02
Colombia	0.76	1.62	−0.29	1.33	1.24	−0.21	1.04
Northern Europe	0.82	0.67	−0.91	−0.23	0.58	−0.73	−0.15
Estonia	1.12	0.48	−0.75	−0.27	0.59	−0.81	−0.22
Finland	1.14	0.65	−0.66	−0.01	0.79	−0.72	0.08
Ireland	0.62	0.45	−1.37	−0.92	0.29	−0.84	−0.55
Sweden	0.91	0.88	−0.77	0.12	0.86	−0.68	0.18
UK	0.73	0.78	−1.01	−0.23	0.59	−0.72	−0.13
Central Europe	0.89	3.17	−0.69	2.48	2.93	−0.61	2.32
Czech Republic	0.93	1.59	−0.59	1.00	1.52	−0.54	0.98
France	0.86	3.84	−0.75	3.09	3.40	−0.63	2.76
Moldova	0.97	2.62	−0.71	1.91	2.67	−0.67	2.00
Switzerland	0.91	2.57	−0.56	2.01	2.41	−0.50	1.91
Southern Europe	0.92	4.32	−0.72	3.60	4.09	−0.65	3.44
Italy	0.88	4.85	−0.68	4.17	4.43	−0.59	3.84
Portugal	0.79	2.17	−1.32	0.86	1.79	−1.03	0.76
Spain	0.93	4.73	−0.63	4.10	4.53	−0.58	3.95
Middle-East Asia	1.05	2.93	−1.78	1.15	3.25	−1.84	1.41
Iran	1.05	2.93	−1.78	1.15	3.25	−1.84	1.41
East Asia	0.90	0.90	−0.77	0.13	0.84	−0.68	0.16
China	1.02	1.46	−0.89	0.58	1.55	−0.89	0.66
Japan	0.86	0.73	−0.76	−0.03	0.65	−0.64	0.01
South Korea	0.94	0.70	−0.53	0.17	0.69	−0.49	0.19
Southeast Asia	0.78	5.29	−0.84	4.46	4.28	−0.63	3.64
Philippines	0.67	9.15	−0.97	8.18	6.27	−0.61	5.66
Taiwan	0.68	2.83	−1.13	1.70	2.00	−0.75	1.24
Thailand	0.80	4.39	−0.72	3.67	3.62	−0.55	3.07
Vietnam	0.71	11.82	−1.48	10.34	8.64	−1.02	7.62
Australia	0.70	1.02	−1.34	−0.32	0.73	−0.93	−0.21
Australia	0.70	1.02	−1.34	−0.32	0.73	−0.93	−0.21

and vulnerability indices, we calculated R^2 values, measures of explained variations, for various models (see Supplementary Table S5). According to the R^2 value, variation in heat vulnerability explained 95.4% of the variation in total mortality. Supplementary Figs. S10 (region) and S11 (country) show the total temperature-attributable excess mortality with respect to global CO_2 concentration increase, and Table 1 summarizes all descriptive indices for regions and countries.

3.3. Feature selection and index modeling

To analyze whether location-specific factors affecting temperature increase index, we performed multiple nonlinear regressions using location-specific daily temperature range, daily mean temperature, and distance to the nearest coast. Based on the full brute-force feature selection method, all three factors were selected for modeling. Fig. 3a–c demonstrates how the three factors affected the temperature increase index. We observed that regional daily temperature range is strongly and almost linearly related to the temperature increase index (Fig. 3a). In addition, for cold regions with mean daily temperature below 10 °C, a lower mean daily temperature indicates a higher temperature increase index (Fig. 3b). In Fig. 3c, the temperature increase index stays nearly constant below 10 km and increases with logarithm of the distance to the nearest coast above 10 km. To quantify the above relationship, we calculated the amount of increase in the index with respect to the interquartile-range (IQR) increase of factors (see Supplementary Table S6). The IQR increase of daily temperature range, logarithm of distance to the nearest coast, and daily mean temperature increased the index by 0.166, 0.102 and 0.007 °C/100 ppm/IQR, respectively. Fig. 3d compares the temperature increase index and the modeled temperature increase index based on the above three factors. The R^2 value of the model is 0.76.

For modeling heat and cold vulnerability indices, we performed multiple linear regression based on location-specific daily temperature range, daily mean temperature, and distance to the nearest coast, and country-specific population below poverty line, population aged 65 and over, population with obesity, and the total health expenditure per capita. Based on the full brute-force feature selection, daily temperature range and population aged 65 and over were dropped for modeling heat and cold vulnerability indices, respectively. Fig. 4a–f demonstrates the relationship between the heat vulnerability index and various factors, Fig. 5a–f demonstrates the relationship between the cold vulnerability indices and various factors, and Supplementary Table S6 shows the increase of the indices with respect to the IQR increase of factors. We found that health expenditure, obese population proportion, and elderly population proportion affected the heat vulnerability index most by −3.859, 2.608, and 2.055%p/°C/IQR, respectively, while obese population proportion, daily temperature range, and mean daily temperature affected the cold vulnerability index most by 0.278, 0.176, and 0.152%p/°C/IQR. Figs. 4g and 5g demonstrate how well the heat and cold vulnerability indices were modeled, respectively. As can be seen, these indices were not well modeled, and the corresponding R^2 values were only 0.36 and 0.39 for heat and cold vulnerabilities, respectively. Such low R^2 values were partly due to the absence of location-specific information for demographic and socio-economic variables we used.

4. Discussion

4.1. Interpretation of relationships between indices and location-specific factors

The temperature increase index increased almost linearly with the temperature range (Fig. 3a). This can be attributed to the activity of water hindering the temperature change. The regions with small temperature range are typically tropical rainforest regions or coastal

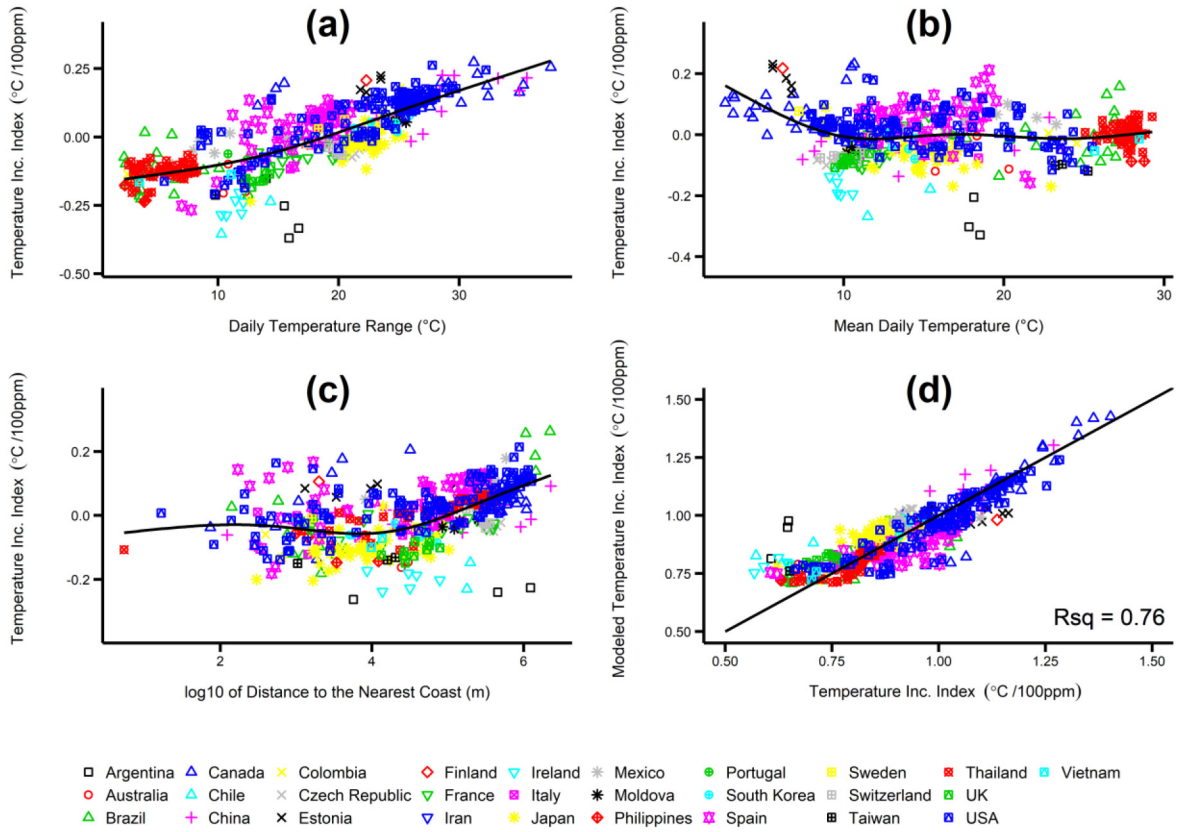

Fig. 3. Modeling for temperature increase index. Relationship between the index and (a) daily temperature range, (b) mean daily temperature, and (c) log10 of distance to the nearest coast. (d) Comparison of the temperature increase index and the model result.

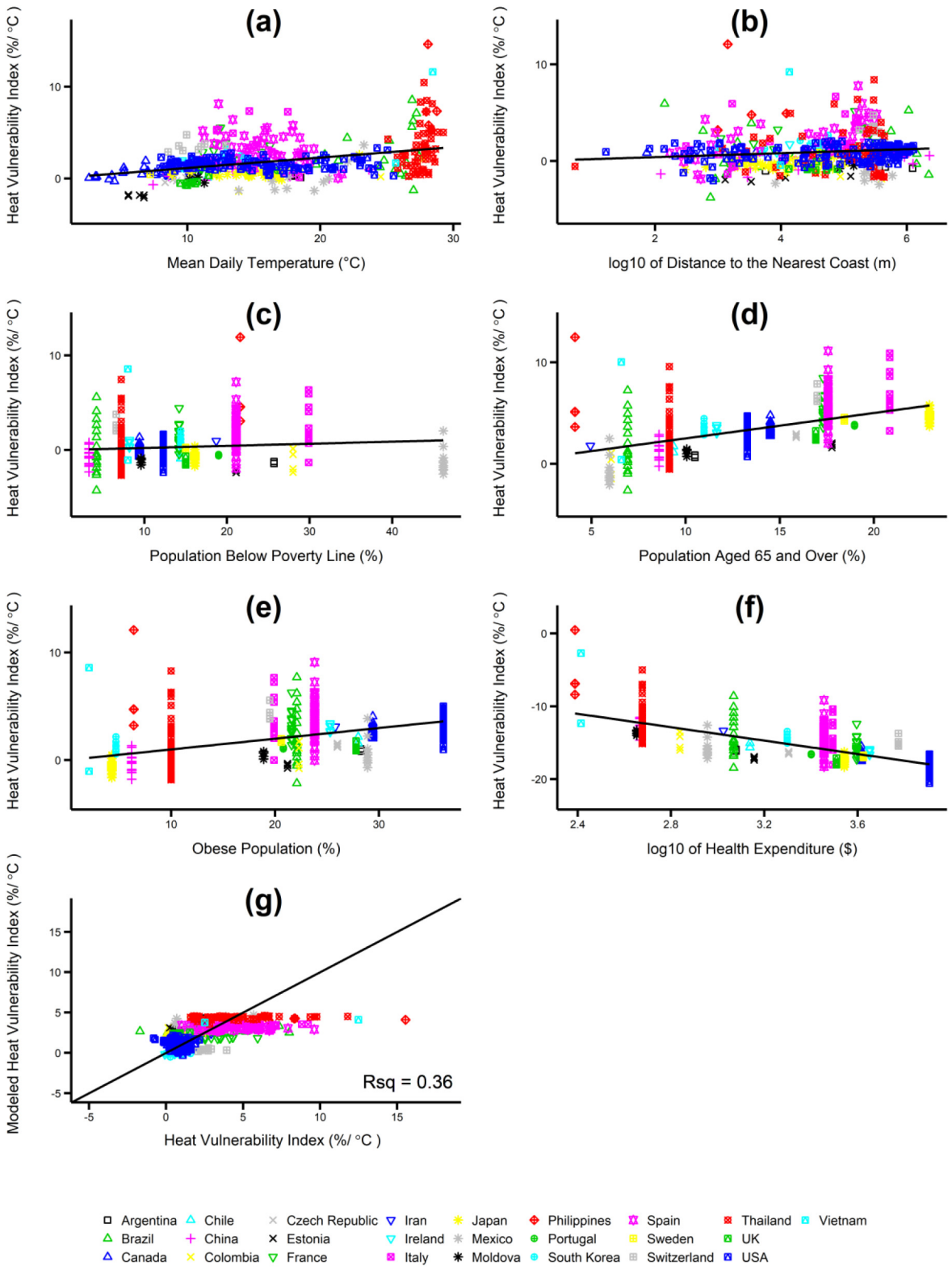

Fig. 4. Modeling for heat vulnerability index. Relationship between the index and (a) mean daily temperature, (b) log10 of distance to the nearest coast, (c) population below poverty line, (d) population aged 65 and over, (e) obese population, and (f) log10 of health expenditure. (g) Comparison of the heat vulnerability index and the model result.

regions, where water is abundant. This water will evaporate and absorb energy that would otherwise increase atmospheric temperature, thereby lowering the temperature increase index. The higher thermal mass of water compared with land is another reason for low index. The relationship between daily mean temperature and the temperature increase index observed in cold regions with mean daily temperature below 10 °C (Fig. 3b) can be attributed to the fact that increased temperature in such cold regions reduces snow and ice. This exposes darker surface and absorbs more sunlight, thereby adding additional warming effect. Dependence of the temperature increase index on the distance to

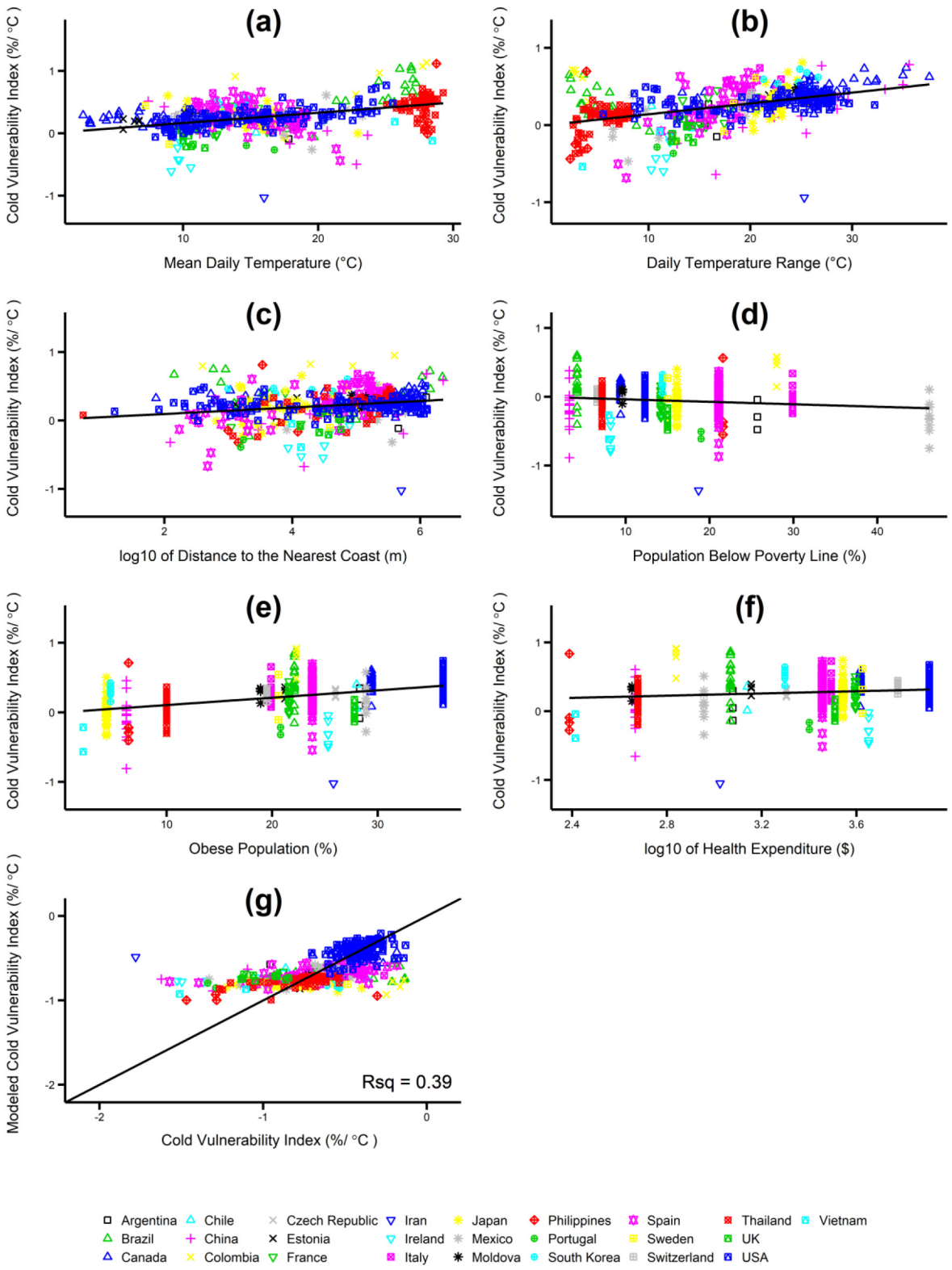

Fig. 5. Modeling for cold vulnerability index. Relationship between the index and (a) mean daily temperature, (b) daily temperature range, (c) log10 of distance to the nearest coast, (d) population below poverty line, (e) obese population, and (f) log10 of health expenditure. (g) Comparison of the cold vulnerability index and the model result.

the nearest coast (Fig. 3c) can be similarly attributed to less evaporation and smaller thermal mass in regions far from sea. A comprehensive physical science basis of climate change can be found in a report by IPCC (2013).

The heat vulnerability index showed a large negative dependence on the total health expenditure per capita, while it showed a large positive dependence on proportions of obese and elderly populations (Fig. 4d–f). This can be understood since the health expenditure per capita represents the quality of health care that makes people less vulnerable and the obese and elderly populations were more vulnerable

to extreme heat than the overall population. However, unlike obese and elderly populations, population below poverty line does not exhibit any strong relationship with the vulnerability index.

4.2. Advantage of index-based health burden analysis

In this work, we quantified the global health burden of 459 locations based on three indices, temperature increase, vulnerability, and mortality increase. The values of these indices were not uniform across the globe. To understand the variability, we performed a multiple regression with the indices being dependent variables.

An advantage of this work is that the descriptive indices are easier to read and utilize than a conventional representation comprised of multiple mortality values projected for multiple climate scenarios and projection periods (e.g., in 2030s, 2060s, and 2090s). Descriptive indices are simple in format, by combining information from multiple scenarios and a wider range of projection period. Such characteristics are useful in summarizing and comparing the results from a large number of study locations.

Second, the temperature and mortality increase indices directly show impacts of climate change with respect to the global CO_2 concentration increase, a main culprit of the climate change. By definition, the indices can provide guidance for the setting of a carbon budget, to limit the temperature or mortality increase to certain targets.

5. Limitations and future works

The descriptive indices used in this work were based on linear regressions. However, there are temperature increase, vulnerability, and mortality increase characteristics that cannot be captured by linear regressions. The temperature increase with respect to global CO_2 increase shows slightly diminishing slope with higher CO_2 concentrations, while heat vulnerability trend shows slightly increasing slope with higher temperature. Such nonlinearity is lost with descriptive index representation. However, we chose linear modeling over the nonlinear modeling to keep the index simple in format due to the abovementioned advantages. In addition, we think these indices represent the overall curve well enough for comparison and modeling. However, researchers should consider the advantages and disadvantages to various methods including the use of conventional time-series or index representations for their analysis.

For predicting the future mortality, we assumed no adaptation and used the baseline temperature-mortality relationships throughout the study period. There are no widely accepted approaches to predict the future relationship between temperature and health and to estimate how this relationship will change over time (World Health Organization (WHO), 2014). However, such estimates are likely to differ due to advancements in medical treatment, air-conditioning, housing standards, and risk communications and other socio-economic and behavioral changes (Orru et al., 2018). Therefore, the future mortality predicted here might be overestimated. In addition, we did not consider changes in the population or its composition. Studies have shown that the elderly population is more vulnerable to temperature increase than the younger population (Lee and Kim, 2016). Therefore, given the global trend of an aging society, the future mortality may be underestimated. While this study considered regional vulnerability, there are other vulnerabilities specific to gender, age group, and socio-economic status such as income level and educational attainment. Future work could investigate these cohort-specific vulnerabilities.

In modeling, this study used three meta-information for temperature increase index and seven meta-information for vulnerability indices. These are important variables in describing climatic, geographic, demographic and socio-economic characteristics of each location. However, to better understand the regional variability in temperature and health risks, future studies should gather a larger number of meta-variables in categories of climate, geography, demography, socio-economy and policy. In addition, this study used data from 459 locations in 28 countries in 10 continental regions. The spatial coverage of the data varies from country to county and from continent to continent. For example, we used 133 locations in USA and 56 locations in Thailand, while we used only one location each in Finland and Iran (see Supplementary Table S2). Therefore, future studies are needed using mortality and temperature data with more spatial coverage and with other less studied locations (e.g., Africa, India, and Russia) to obtain a more comprehensive estimate of global health burden.

6. Conclusions

In this study, we projected future mortality due to temperature increase in 459 locations worldwide under RCP scenarios. We introduced three descriptive indices to summarize the temperature increase and health burden in a format that is easy to read and utilize. These indices can be useful to obtain a different perspective of the effect of the climate change by reporting increment in excess mortality by measures of warming, greenhouse gas emissions and concentrations, rather than by time under specific scenarios. Based on three indices, we compared the amounts of temperature and mortality increases across locations. Among studied locations, tropical countries such as the Philippines, Vietnam, and Thailand are at higher mortality risk when temperature increases. In addition, we analyzed the factors affecting the temperature and mortality increase based on multiple regression. The regression analysis confirmed that the amount of temperature increase projected by GCM is strongly correlated with the increasing distance from the coast and the increasing daily temperature range and that the total health expenditure per capita, obese and elderly population proportions are the major factors affecting vulnerability to temperature increase.

Declaration of Competing Interest

The authors declare that they have no known competing financial interests or personal relationships that could have appeared to influence the work reported in this paper.

Acknowledgement

This study was supported by the Global Research Lab (#K21004000001-10A0500-00710) through the National Research Foundation of Korea (NRF), funded by the Ministry of Science, ICT (Information and Communication Technologies), and Future Planning. JL was supported by the National Research Foundation of Korea as NRF-SNSF Researcher Exchange Program (NRF-2018K2A9A1A06086694). AG was supported by Medical Research Council UK (Grant ID: MR/M022625/1) and Natural Environment Research Council UK (Grant ID: NE/R009384/1). JK and AU were supported by the Czech Science Foundation, project no. 18-22125S. HO and EI were supported by the Estonian Ministry of Education and Research (Grant no IUT34-17). JJKJ and NRIR were supported by the Research Council for Health, Academy of Finland (Grant no 266314 and 310372). MH and YH were supported by the Environment Research and Technology Development Fund (S-14) of the Environmental Restoration and Conservation Agency. AT was supported by the Japan Society for the Promotion of Science (JSPS) Invitational Fellowships for Research in Japan (S18149).

Appendix A. Supplementary data

Supplementary data to this article can be found online at https://doi.org/10.1016/j.envint.2019.105027.

References

Akaike, H., 1974. A new look at the statistical model identification. IEEE Trans. Autom.

Control 19 (6), 716–723.
Bai, L., et al., 2016. Hospitalizations from hypertensive diseases, diabetes, and arrhythmia in relation to low and high temperatures: population-based study. Sci. Rep. 6, 30283.
Błażejczyk, et al., 2013. Forecast changes for heat and cold stress in Warsaw in the 21st century, and their possible influence on mortality risk. Papers on Global Change 20, 47–62.
Gasparrini, A., Armstrong, B., Kenward, M.G., 2010. Distributed lag non-linear models. Stat. Med. 29, 2224–2234.
Gasparrini, A., Armstrong, B., Kenward, M.G., 2012. Multivariate meta-analysis for non-linear and other multi-parameter associations. Stat. Med. 31, 3821–3839.
Gasparrini, A., et al., 2015. Mortality risk attributable to high and low ambient temperature: a multicountry observational study. Lancet 386, 369–375.
Gasparrini, A., et al., 2017. Projections of temperature-related excess mortality under climate change scenarios. Lancet Planet Health 1, e360–e367.
Guo, Y., Li, S., Liu, D.L., Chen, D., Williams, G., Tong, S., 2016. Projecting future temperature-related mortality in three largest Australian cities. Environ. Pollut. 208, 66–73.
Hajat, et al., 2014. Climate change effects on human health: projections of temperature-related mortality for the UK during the 2020s, 2050s and 2080s. J. Epidemiol. Community Health 68, 641–648.
Hempel, S., Frieler, K., Warszawski, L., Schewe, J., Piontek, F., 2013. A trend-preserving bias correction—the ISI-MIP approach. Earth Syst. Dynam. 4, 219–236.
Higgins, J.P.T., Thompson, S.G., 2002. Quantifying heterogeneity in a meta-analysis. Stat. Med. 21 (11), 1539–1558.
Intergovernmental Panel on Climate Change (IPCC), 2007. Climate Change 2007: Synthesis Report.
Intergovernmental Panel on Climate Change (IPCC), 2013. Climate Change 2013: The Physical Science Basis. Contribution of Working Group I to the Fifth Assessment Report of the Intergovernmental Panel on Climate Change. Cambridge University Press, Cambridge, United Kingdom and New York, NY, USA 1535 pp.
Lee, J.Y., Kim, H., 2016. Projection of future temperature-related mortality due to climate and demographic changes. Environ. Int. 94, 489–494.
Lee, J.Y., Choi, H., Kim, H., 2018. Dependence of future mortality changes on global CO_2 concentrations: a review. Environ. Int. 114, 52–59.
Li, T., Horton, R.M., Kinney, P.L., 2013. Projections of seasonal patterns in temperature-related deaths for Manhattan, New York. Nat. Clim. Chang. 3, 717–721.
Liu, L.Q., et al., 2011. Associations between air temperature and cardio-respiratory mortality in the urban area of Beijing, China: a time-series analysis. Environ. Health 10, 51–61.
Martin, S.L., Cakmak, S., Hebbern, C.A., Avramescu, M.-L., Tremblay, N., 2012. Climate change and future temperature-related mortality in 15 Canadian cities. Int. J. Biometeorol. 56, 05–619.
Orru, K., Tillmann, M., Ebi, K.L., Orru, H., 2018. Making administrative systems adaptive to emerging climate change-related health effects: case of Estonia. Atmosphere 9 (6), 221.
Patz, J.A., McGeehin, M.A., Bernard, S.M., Ebi, K.L., Epstein, P.R., Grambsch, A., Gubler, D.J., et al., 2000. The potential health impacts of climate variability and change for the United States: executive summary of the report of the health sector of the U.S. National Assessment. Environ. Health Perspect. 108 (4), 367–376.
Schwartz, J.D., Lee, M., Kinney, P.L., Yang, S., Mills, D., Sarofim, M.C., Jones, R., Streeter, R., St Juliana, A., Peers, J., Horton, R.M., 2015. Projections of temperature-attributable premature deaths in 209 U.S. cities using a cluster-based Poisson approach. Environ. Health 14, 85.
Seneviratne, S.I., Donat, M.G., Pitman, A.J., Knutti, R., Wilby, R.L., 2016. Allowable CO_2 emissions based on regional and impact-related climate targets. Nature 529, 477–483.
Tobias, A., Armstrong, B., Gasparrini, A., 2017. Investigating uncertainty in the minimum mortality temperature methods and application to 52 Spanish cities. Epidemiology 28 (1), 72–76.
Vardoulakis, et al., 2014. Comparative assessment of the effects of climate change on heat- and cold-related mortality in the United Kingdom and Australia. Environ. Health Perspect. 122 (12), 1285–1292.
Warszawski, L., Frieler, K., Huber, V., Piontek, F., Serdeczny, O., Schewe, J., 2014. The Inter-Sectoral Impact Model Intercomparison Project (ISI-MIP): project framework. Proc. Natl. Acad. Sci. 111, 3228–3232.
Wood, S.N., 2006. Generalized Additive Models: An Introduction With R. Chapman & Hall/CRC press.
World Health Organization (WHO), 2014. Quantitative Risk Assessment of the Effects of Climate Change on Selected Causes of Death, 2030s and 2050s. prepared by. Public Health & Environment Department, Health Security & Environment Cluster of World Health Organization.